



Impact of Geospatial Data Enhancements for Regional-Scale 2D Hydrodynamic Flood Modeling: Case Study for the Coastal Plain of Virginia

Mohamed M. Morsy, Ph.D.¹; Natalie R. Lerma²; Yawen Shen, Ph.D.³; Jonathan L. Goodall, Ph.D., P.E., F.ASCE⁴; Chris Huxley⁵; Jeffrey M. Sadler, Ph.D.⁶; Daniel Voce⁷; Gina L. O'Neil, Ph.D.⁸; Iman Maghami⁹; and Faria T. Zahura¹⁰

Abstract: Hydrology in low-relief coastal plains is especially challenging to simulate in flood modeling applications. Two-dimensional (2D) hydrodynamic models are often necessary, but creating such models for regional-scale systems at a high spatial resolution presents significant data challenges. The objective of this research is to explore these challenges using a 2D hydrodynamic model built for a 5,800-km² region in the coastal plain of Virginia as a case study. Systematic enhancements to the hydrodynamic model's topographic, bathymetric, streamline, surface roughness, and rainfall representations are tested to assess their impact on the model's predictive skill. Results showed that incorporating high-resolution terrain and land use data sets alone only produced minor improvements to model accuracy. However, the addition of river cross-section data collected through site visits and careful, detailed quality control (QC) of observed rainfall data produced much more substantial improvements to accuracy. Based on these findings, increased focus should be placed on integrating topographic and river bathymetric data sets for low-relief coastal plain regions along with improved methods for QC of observed rainfall data, especially for extreme weather events. **DOI: 10.1061/(ASCE)HE.1943-5584.0002065.** © 2021 American Society of Civil Engineers.

Author keywords: Two-dimensional (2D) hydrodynamic modeling; Regional-scale hydrologic modeling; Flood forecasting; Flood resilience; Coastal flooding.

Introduction

Recent storms have caused significant flooding to coastal plain communities, and these flooding events are expected to increase in frequency and intensity under changing climate conditions (Feng et al. 2016; Prein et al. 2017). In the US, Hurricanes Harvey and Irma, which occurred back to back in 2017, were part of one of the most active Atlantic hurricane seasons (NOAA 2017). These hurricanes caused both fatalities and significant damage, largely due to rainfall-driven flooding (Bacopoulos 2019). Hurricane Florence, which struck the US East Coast in 2018, caused widespread

power outages and devastating damage due to significant rainfall, a storm surge, and high wind speeds; these rainfall also caused significant flooding throughout the coastal plain (NOAA 2018). With such events becoming more frequent in the coming years, there is an increased need to better forecast rainfall-driven flooding impacts at a high spatial resolution to mitigate impacts and to assist in recovery efforts.

Efforts to improve rainfall-driven flood forecast modeling often use computationally efficient one-dimensional (1D) river hydraulic models (Kalyanapu et al. 2011; Timbadiya et al. 2015). For example, one key effort in the US for improved flood forecasting is the

¹Assistant Professor, Irrigation and Hydraulics Engineering Dept., Faculty of Engineering, Cairo Univ., P.O. Box 12211, Giza 12614, Egypt; Project Water Resources Engineer, Dewberry, 8401 Arlington Boulevard, Fairfax, VA 22031-4666. Email: mohamedmorsyanwar@cu.edu.eg; mmorsy@dewberry.com

²Graduate Research Assistant, Dept. of Engineering Systems and Environment, Univ. of Virginia, 151 Engineers Way, P.O. Box 400747, Charlottesville, VA 22904-4747. Email: nrl5fh@virginia.edu

³Graduate Research Assistant, Dept. of Engineering Systems and Environment, Univ. of Virginia, 151 Engineers Way, P.O. Box 400747, Charlottesville, VA 22904-4747. Email: ys5dv@virginia.edu

⁴Professor, Dept. of Engineering Systems and Environment, Associate Director, Link Lab, Univ. of Virginia, 151 Engineers Way, P.O. Box 400747, Charlottesville, VA 22904-4747 (corresponding author). ORCID: https://orcid.org/0000-0002-1112-4522. Email: goodall@virginia.edu

Note. This manuscript was submitted on June 4, 2020; approved on November 20, 2020; published online on January 27, 2021. Discussion period open until June 27, 2021; separate discussions must be submitted for individual papers. This paper is part of the *Journal of Hydrologic Engineering*, © ASCE, ISSN 1084-0699.

⁵Principal Engineer and Software Business Development Lead, BMT WBM Pty Ltd., Level 8, 200 Creek St., Brisbane, QLD 4000, Australia.

⁶Graduate Research Assistant, Dept. of Engineering Systems and Environment, Univ. of Virginia, 151 Engineers Way, P.O. Box 400747, Charlottesville, VA 22904-4747; Currently, Research Hydrologist, US Geological Survey, 8505 Research Way, Middleton, WI 53562. ORCID: https://orcid.org/0000-0001-8776-4844

⁷Undergraduate Research Assistant, Dept. of Engineering Systems and Environment, Univ. of Virginia, 151 Engineers Way, P.O. Box 400747, Charlottesville, VA 22904-4747; Currently, Developer, Palo Alto Networks, 3000 Tannery Way, Santa Clara, CA 95054.

⁸Graduate Research Assistant, Dept. of Engineering Systems and Environment, Univ. of Virginia, 151 Engineers Way, P.O. Box 400747, Charlottesville, VA 22904-4747; Currently, Technical Consultant, Environmental Systems Research Institute, 167 S. Taylor Ave., Louisville, CO 80027-3025.

⁹Graduate Research Assistant, Dept. of Engineering Systems and Environment, Univ. of Virginia, 151 Engineers Way, P.O. Box 400747, Charlottesville, VA 22904-4747. Email: im3vp@virginia.edu

¹⁰Graduate Research Assistant, Dept. of Engineering Systems and Environment, Univ. of Virginia, 151 Engineers Way, P.O. Box 400747, Charlottesville, VA 22904-4747. Email: fz7xb@virginia.edu National Water Model (NWM), which uses the Weather Research and Forecasting Hydrologic model (WRF-Hydro). WRF-Hydro is configured to use the Noah-MP land surface model (LSM) and a 1D Muskingum-Cunge channel routing procedure (Office of Water Prediction 2019). Muskingum-Cunge routing assumes uniform water velocity and a constant water surface elevation modeled at each cross section (Bates and De Roo 2000; Crowder and Diplas 2000; García et al. 2015). These assumptions are appropriate and widely used in flood forecasting applications in areas of the US that have sufficient topographic relief (Bedient et al. 2008; Kalyanapu et al. 2011; Knebl et al. 2005; Noman et al. 2001; Shrestha and Nestmann 2009; Tate et al. 2002; Yan et al. 2015). However, they are often not appropriate for low-relief regions like coastal plains with more complex flow structures (Bates et al. 1992; Leandro et al. 2009).

Hydrodynamic models can simulate the two-dimensional Saint-Venant equations and provide flow field descriptions that are a better alternative for these low-relief terrains (Engineers Australia 2012; National Research Council 2009; Timbadiya et al. 2015). However, there are data and computational challenges with using two-dimensional (2D) models that have limited their widespread adoption in practice (Lamb et al. 2009). Researchers have focused on approaches to improve the computation time of 2D hydrodynamic models, including applying new numerical schemes and parallel computing (Yu 2010). Others have leveraged advances in cloud computing and graphical processing units (GPUs) to address computational challenges (Morsy et al. 2018). These advances are making 2D models for flood forecasting applications more practical.

At the same time, advances in geospatial and remote sensing data are providing more detailed representations of the landscape needed for constructing accurate 2D hydrodynamic models. A key focus of prior research has been on leveraging the now widely available high-resolution topographic data collected using lidar to capture the land surface within 2D hydrodynamic models. For example, Marks and Bates (2000) compared standard parametrization methods of 2D hydraulic models with high-resolution lidar. They found that even small topography changes can affect flood hydraulics, thus producing different percentages and patterns of inundation. Still, significant terrain processing such as filtering, modeling systemic errors, feature detection, and thinning must be applied to these data before they can be used in hydrodynamic models (Abdullah et al. 2012). Just selecting a filtering algorithm for terrain processing can be quite difficult, as Abdullah et al. (2012) highlight. Once selected, these filtering and quality control measures can consume an estimated 60%-80% of processing time (Schumann et al. 2008). In another study, an algorithm was developed for identifying features such as short and tall vegetation in lidar data (Cobby et al. 2001). For estuaries and bays, Muñoz et al. (2020) developed and used an Arc-GIS version 10.1 tool to correct digital elevation models (DEMs) using updated emergent herbaceous wetlands regions for improved model maximum floodwater height (MFH) and velocity (MFV). Ensuring the compatibility of the topographic resolution and the computational resolution is yet another challenge (Bates et al. 2003).

Prior research using 2D hydrodynamic models for flooding has also explored parameterization, especially for critical parameters like roughness coefficients (Lim and Brandt 2019; Liu et al. 2019), distributed rainfall representations (Bruni et al. 2015; Ochoa-Rodriguez et al. 2015), and other factors critical to accurate flood forecasting (Zhao et al. 2013). For example, Manning's coefficient is often used for parameterizing roughness. Although standard tables of Manning's values are widely available and have been used for decades to assign reasonable roughness values in 1D models (Chow 1959), applying these values directly to 2D models may result in inaccurate model outputs (Horritt et al. 2006). Lim and

Brandt (2019) and Liu et al. (2019) found that models with highresolution DEMs perform better when their roughness values are decreased from the standard recommendations, while models with low-resolution DEMs perform better when their roughness values are increased from the standard recommendations. In another study by Medeiros et al. (2012), in situ Manning's roughness values were found to vary significantly from those prescribed using standard land use/land cover (LULC) methods. Thus, more research is needed to better understand how different improvements to such models influence their accuracy.

While this past research has focused primarily on topographic and surface roughness improvements to 2D hydrodynamic models, less work has focused on other data improvements including river bathymetry and accurate rainfall forcing data. The objective of this research is to systematically explore these data enhancements to understand how they impact the predictive skill of a 2D hydrodynamic model for a case study region. This study builds on prior research applying a particular 2D hydrodynamic model, TUFLOW version 2016-03, to a region of the coastal plain of Virginia to provide flood risk prediction of transportation infrastructure during severe storm events (Morsy et al. 2018). The goal of this research is to best direct time-consuming, expensive data collection and processing efforts to those that will be most impactful in creating a more accurate 2D hydrodynamic model.

Materials and Methods

Study Area

The study area is the portion of the Chowan River Basin in the coastal plain of Virginia (Fig. 1). The 2D model domain of the study area is about 5,800 km² and includes the Nottoway, Blackwater, and Meherrin Rivers. The study area's longest flow path is about 180 km, with a slope varying from 21% in the higher-relief western portion of the study domain to nearly level in the lowerrelief eastern portion of the study domain. The contributing subwatersheds upstream of the study area (an additional ~5,200 km²) consist of high-relief terrain areas. These subwatersheds can be adequately modeled using a lumped water-scale hydrologic model [e.g., either the Hydrologic Engineering Center-Hydrologic Modeling System (HEC-HMS) model or the NWM] to provide inflow boundary conditions for the 2D hydrodynamic model, TUFLOW. The outlet is located downstream from where the Nottoway, Blackwater, and Meherrin Rivers merge into the Chowan River approximately 80.5 km (50 mi) from the Albemarle Sound. Downstream outlet boundary conditions were assumed not to be influenced by tidal conditions and water backflows associated with tides in this study because the watershed outlet is dominated by rainfall and runoff, especially during flooding events. A report from the USGS states that while tidal influence may extend to the lower portions of tributaries to the Chowan River, most water fluctuations are minimal due in large part to its distance from the ocean (Giese et al. 1985).

Original Model

The 2D hydrodynamic TUFLOW model used as the original model in this study is described in detail in Morsy et al. (2018). The model included a 10-m-resolution DEM from the National Elevation Dataset (NED), county-scale soil data (SSURGO 2018), and 30-m-resolution land use data from the 2011 National Land Cover Dataset (USGS 2011) used to derive roughness coefficients within the model. The model also included the location of 493 georeferenced bridges and culverts owned and operated by the Virginia Department of Transportation (Virginia DOT), each with survey roadway

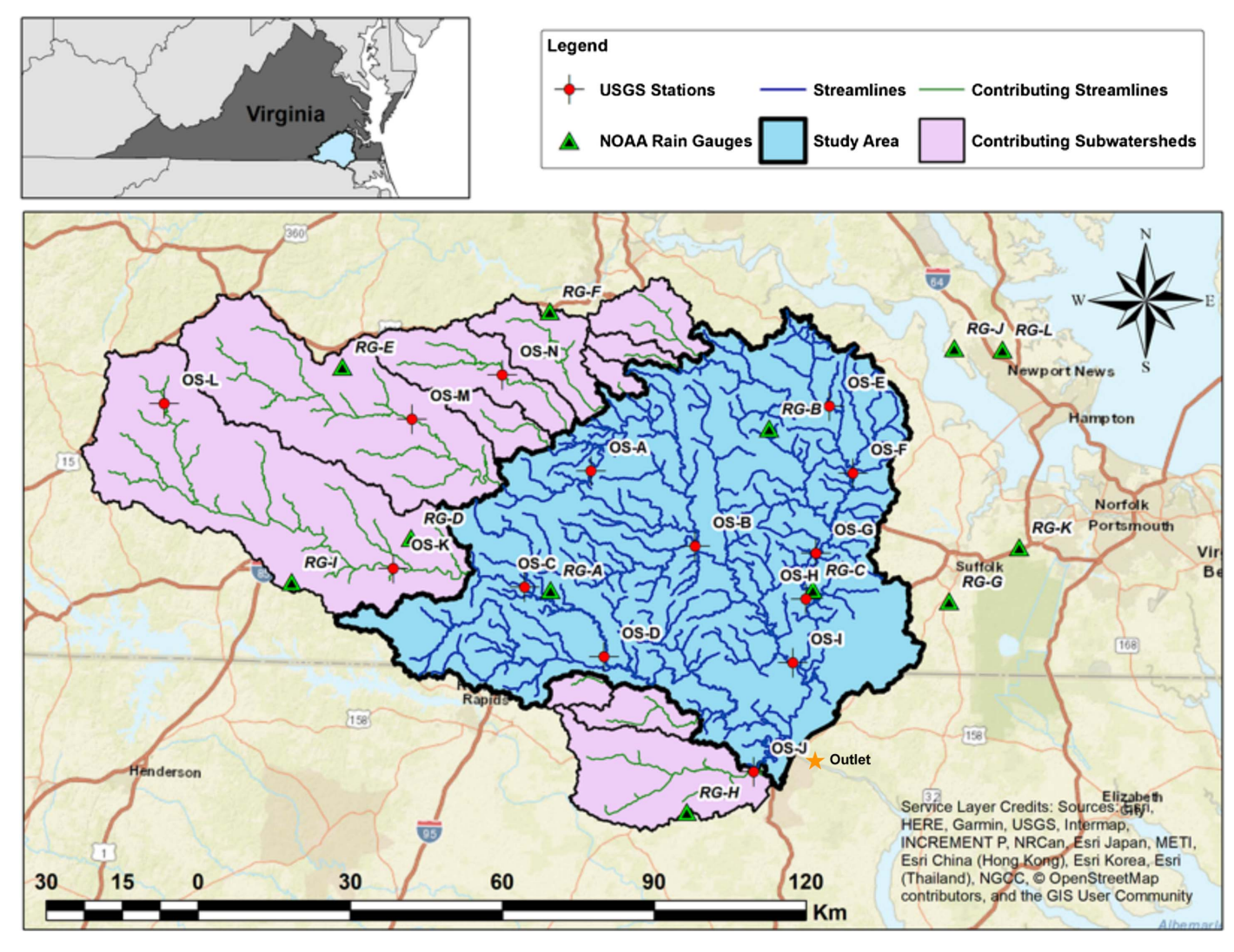


Fig. 1. Study and contributing areas for water depths and flows simulated by the 2D hydrodynamic model. [Map data from ESRI, HERE, Garmin, USGS, Intermap, INCREMENT P, NRCan, ESRI Japan, METI, Esri China (Hong Kong), Esri Korea, Esri (Thailand), NGCC, © OpenStreetMap contributors, and the GIS User Community.]

elevations that can be used for estimating flood inundation. Throughout this study, the computational cell resolution was a 30-m fixed-grid resolution, with 6.4 million computational cells as further described in Morsy et al. (2018).

Two different real-time rainfall products were used by the system for hindcasting applications to calibrate and evaluate the model: (1) National Oceanic and Atmospheric Administration (NOAA) gauges, and (2) Next Generation Weather Radar (NEXRAD) rainfall estimates. The model was calibrated and evaluated against historical water elevation data measured by USGS with the goal of matching the modeled water elevation peaks rather than the complete stage depth time series for major storm events. This original model could

be considered a basic starting point for any national-scale 2D hydrodynamic flood model given nationally-available geospatial and observational data. The model's enhancements described in the following section represent modifications made to the model to explore their impact on improving the model's accuracy at matching observed water elevations.

Data Enhancements

Table 1 summarizes all enhancements made to the original model to test the model's sensitivity to these input data improvements. Improvements to the model were quantified as a reduction in the

Table 1. Original and final model comparison

Original model

Coarse-resolution DEM data set (10-m DEM)

Missing and inaccurate streamlines
[National Hydrography Dataset Plus (NHDPlus)
and 10-m DEM]

Coarse-resolution land use data set (30-m LULC)

Sparse rain gauge observations, use of tropical rainfall measuring mission (TRMM)

Higher-resolution data sets used where available (1-m DEM) for low-relief terrain Site visits for river cross-section bathymetric data to improve streamlines

Final model

30-m LULC with 3-m resolution near channels and in floodplain Improved rain gauging network and quality control of rainfall data before interpolation

relative error (RE) between observed and modeled water elevation and improvement in the model's Nash-Sutcliffe model efficiency coefficient (NSE). NSE values can range from $-\infty$ to 1, with an NSE value of 1 indicating a perfect match between the modeled outputs and the observed data (McCuen et al. 2006). The model is generally considered a well-calibrated model of sufficient quality when the NSE value is at least 0.5 (Moriasi et al. 2007, 2015; Ritter and Muñoz-Carpena 2013).

Terrain

The original model used a 10-m-resolution DEM for representing the terrain within the study domain. High-resolution lidar-derived DEMs (from 0.76 to 1.52 m in horizontal resolution) are available for most of the study region (VGIN 2016a). The small portion of the study region not covered by these high-resolution lidar data and for which the 10-m DEM was used, fortunately, has higher topographic relief. For consistency across the study area, the various DEMs were resampled to a domain-wide 1-m DEM.

Given that the model's primary application is to forecast flooding impacts on transportation infrastructure, it was particularly important to represent channel cross sections at bridges and culverts. To do this, it was first necessary to obtain accurate road centerlines in the study domain from the Virginia Geographic Information Network (VGIN). Using a georeferenced data set of bridges and culverts provided by Virginia DOT, it was possible to identify the road segments representing each bridge and culvert. Next, the road segment crossing the flow path was extended to cover the entire floodplain at that bridge or culvert. Finally, elevation values were extracted from the 1-m DEM from across this road segment centerline to capture the channel cross section at the bridge or culvert location. Typical airborne, terrestrial lidar may be unable to capture the bathymetric portion of a channel cross section because it typically operates with near-infrared (NIR) wavelengths (typically 1,064-nm lasers), which cannot penetrate water (Fernandez-Diaz et al. 2014; McKean et al. 2009; NOAA 2013). For some bridges that cross larger rivers in the study domain, accurate representation of river cross sections must be obtained through other means, as will be discussed in the section "Channel Cross Section."

Streamlines

The TUFLOW model uses a vector streamline to define a path as well as start and end elevations for each segment for directing channelized flow through the model. The original model's streamlines were compared with aerial imagery for the lowest-relief portion of the study region, showing significant discrepancies and potential sources of error for the original model. The streamlines in the original model were also compared to the National Hydrography Dataset Plus (NHDPlus), revealing that some rivers were missing in the model. A new version of the streamlines was generated to address these potential sources of error, starting with the latest available version of NHDPlus for the study region. There was a mismatch

with the 1-m DEM data set and with areal imagery data for some reaches in the NHDPlus flowlines feature data set. To ensure the alignment of these reaches with the 1-m DEM data set and imagery data, the streamline data were modified through both partial automation and manual modification, with the automation adjustments made using hydrologic terrain processing tools in geographic information system (GIS) software.

Roughness Coefficients

The model's roughness coefficients were obtained from land cover maps and established lookup tables relating land cover types to typical Manning's coefficient values. The original model relied on only the National Land Cover Database (USGS 2011), which has a relatively coarse spatial resolution of 30 m. To improve on this, a second source of land cover data with 3-m spatial resolution, the Virginia Land Cover Database (VLCD) provided by VGIN, was used (VGIN 2016b). Because the 3-m resolution of VLCD 2015 is not required for the entire study area (e.g., outside of river channels and floodplains) and because doing so would significantly increase the computational demands of the model, the National Land Cover Database 2011 was used as the default land cover representation in the study area and VLCD 2015 as the land cover representation in and near (within 1 km) river channels.

From this merged land cover map, Manning's coefficient values were used for each land cover type recommended by Kalyanapu et al. (2009) for defining initial roughness coefficients (Table 2). These roughness coefficients were then adjusted so that the simulated water elevation values better match water elevation values observed at the USGS monitoring stations within the study domain for the Hurricane Matthew storm event. These adjustments were made for the eight dominant land covers in the study domain manually, given the significant model runtime, which prohibited more automated sensitivity and calibration procedures. Table 2 gives the initial and final values of Manning's coefficients for these land cover types.

Channel Cross Section

Channel bathymetry cannot be obtained from typical airborne, topographic lidar because they use NIR wavelengths that do not have enough energy to penetrate water (Fernandez-Diaz et al. 2014; McKean et al. 2009; NOAA 2013). Additionally, bathymetry data are not available for most rivers in the US. Therefore, site visits were conducted to the larger streams with USGS gauging stations located in the lower-relief eastern portion of the study area (i.e., USGS Stations OS-E, OS-F, OS-G, OS-H, and OS-I shown in Fig. 1). Cross-sectional information was collected during these site visits by measuring the distance between the bridge deck and the stream bed. Bridge deck locations, where measurements were taken, were recorded using GPS. The obtained cross-sectional information was then included in the channel information within TUFLOW as the cross-section properties. When available, historical cross-section

Table 2. Modified Manning's coefficient values for different land cover types resulting from the model calibration

Land cover code	Land cover description	Initial Manning's coefficient (n)	Final Manning's coefficient (n)	
41	Deciduous forest	0.360	0.12	
42	Evergreen forest	0.320	0.10	
43	Mixed forest	0.400	0.15	
52	Shrub/scrub	0.400	0.15	
71	Grassland/herbaceous	0.368	0.12	
81	Pasture/hay	0.325	0.10	
82	Crop/vegetation	0.323	0.10	
95	Emergent herbaceous wetlands	0.183	0.15	

Source: Data from Kalyanapu et al. (2009).

Table 3. Rainfall gauges available from NOAA within and nearby the study area

		NOAA station		
ID	Station number	Station name	Start	End
RG-A	72027803704	EMPORIA-GRENVLE RGNL ARPT, VIRGINIA	January 1, 2006	Current date
RG-B	72401993773	WAKEFIELD MUNICIPAL ARPT, VIRGINIA	January 1, 2006	Current date
RG-C	72308313763	FRANKLIN MUNICIPAL-JOHN BEVERLY ROSE AIRPORT, VIRGINIA	October 16, 1994	Current date
RG-D	72077799999	LAWRENCEVILLE BRUNSWICK MUNI, VIRGINIA	June 25, 2014	Current date
RG-E	72401599999	ALLEN C PERKINSON BLACKSTONE AAF/FT PICKETT, VIRGINIA	September 22, 2003	Current date
RG-F	72401493714	DINWIDDIE COUNTY AIRPORT, VIRGINIA	January 1, 2006	Current date
RG-G	72400703719	SUFFOLK MUNICIPAL AIRPORT, VIRGINIA	January 1, 2006	Current date
RG-H	72307993796	TRI-COUNTY AIRPORT, NORTH CAROLINA	January 1, 2006	Current date
RG-I	72411893797	MCKNBRG-BRUNWICK RGNL ARPT, VIRGINIA	January 1, 2006	Current date
RG-J	72308793735	FELKER ARMY AIRFIELD, VIRGINIA	November 1, 1960	Current date
RG-K	72049999999	HAMPTON ROADS EXECUTIVE AIRPORT, VIRGINIA	May 3, 2011	May 20, 2018
RG-L	72308693741	NWPT NEWS/WIMBURG INTL APT, VIRGINIA	January 1, 2000	Current date

surveys for these same bridge locations were obtained from Virginia DOT. The new and historical survey data were then compared to the 1-m DEM data set used by the model, and the channel cross sections were adjusted accordingly. While the inclusion of channel bathymetric data for all large rivers in the model would be ideal, such data are unavailable, so the collected cross-sectional data were used instead.

Rainfall

The original model used TRMM gridded rainfall estimates because NEXRAD estimates were not available for the modeled storm events. Both TRMM and NEXRAD assist in measuring the spatial distribution of rainfall for large domains, such as the one in this study. To improve the spatially distributed rainfall estimates and the temporal resolution of rainfall used by the model, careful analysis and interpolation of gauged rainfall data available within the study region were completed. First, all gauged rainfall data from NOAA gauges in and near the study area were obtained for the modeled storm events (Table 3). Then, by using an inverse distance weight (IDW) interpolation method available within the TUFLOW model with the default exponent of 2 (BMT WBM 2016, p. 655), these 12 rainfall gauges were converted to gridded rainfall data with a 500-m spatial resolution and a 20-min temporal resolution.

Before the rainfall gauge data were interpolated and used in the model, they were first checked for quality control (QC). This QC identified not only rainfall observation outliers but also rain gauge malfunctions during extreme rainfall events. Fig. 2 shows the collected cumulative rainfall data at each of the 12 NOAA gauges

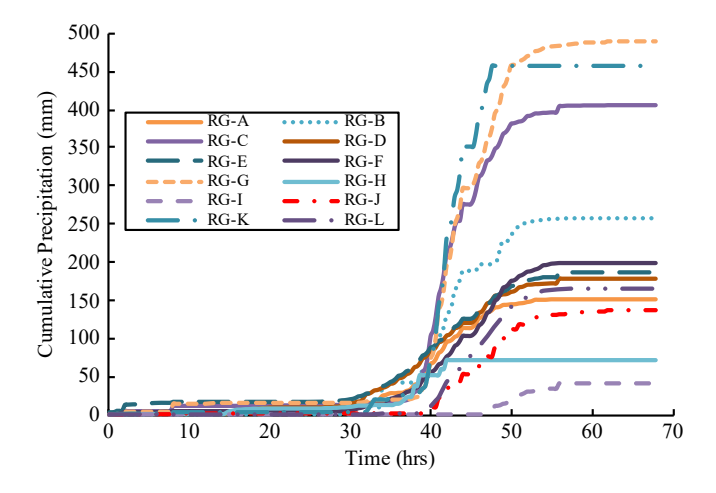


Fig. 2. Cumulative rainfall data at each of the 12 NOAA rainfall gauges for Hurricane Matthew.

identified within the region for Hurricane Matthew. Although there were data available from all 12 NOAA stations for this event, some data had to be disregarded due to what appears to be rain gauge malfunctions. For example, for an extreme rainfall event such as Hurricane Matthew, sudden flat lines in cumulative rainfall data can often mean a gauge, which is often a mechanical tipping bucket, malfunctioned (Skinner et al. 2009; Steiner et al. 1999). This was likely the case with Gauge RG-I, which has significantly lower precipitation values in comparison with another gauge in its proximity (RG-D), and with RG-H, which appears to have failed early in the storm event. The incremental jumps in the RG-J data seems to be unnatural. RG-K has one of the most significant rainfall totals but may have malfunctioned near the end of the event. Based on this analysis, RG-I, RG-J, and RG-K were excluded from the data set used for rainfall interpolation for Hurricane Matthew; data from the nearby gauges RG-D, RG-L, and RG-G were complete and could be referenced in their absence.

Model Evaluation

Model Scenarios

Four different versions of the model inputs were evaluated to better understand the impact of the data enhancements described in the prior section (Table 4). The first version of the model described in the "Original Model" section is referred to as the original model. The second version is the original model enhanced with the new terrain representation, streamlines, and roughness coefficients described in the "Terrain" section through the "Roughness Coefficients" section and is referred to as the new data set model in subsequent sections. The third version builds from the new data set version of the model and further enhances it with improved channel cross-section information obtained through site visits, as described in the section "Channel Cross Section." This version of the model is referred to as the site visit model. Finally, the fourth version of the model represents further enhancements from the site visit model with improved rainfall estimation, as described in the "Rainfall" section, and is referred to as the final model. Even with the use of powerful GPU machines, running the model for the Hurricane Matthew event took approximately 10 h to complete, limiting the variety and combinations of model alternatives that could be tested.

Conducting Model Runs

All test runs for data enhancements to the model were done using Hurricane Matthew. Once data enhancements were complete, the model was evaluated using a second, unnamed storm that occurred on October 11, 2018. The October 11, 2018, storm event had less

Table 4. Model versions tested through this research

Model version name Description			
Original model	Original model as described in the "Original Model" section		
New data set	Original model enhanced with new terrain, new streamlines, and the roughness coefficients		
Site visit	New data set model enhanced through site visits to collect stream cross-section data		
Final model	Site visit model enhanced through improved rainfall estimation		

impact on the study domain than Hurricane Matthew, and therefore it demonstrates the flood warning system's ability to model a less intense storm event. Reynolds et al. (2020) studied the use of single events compared to using multiple or no historical events for model calibration and found that using a single extreme event can significantly improve model predictions compared to those models without historical data. For this reason, and due to the computational demands of the model, we have chosen to use one event for model calibration and an additional event for validation and evaluation. For these evaluation model runs, the input data (inflow boundary conditions and rainfall data) from the NWM were obtained and preprocessed to mimic a run of the flood warning system that would leverage the NWM, rather than HEC-HMS models as described previously, for boundary conditions. The NWM was used for inflow boundary conditions because the NWM output is now available, but was not available before 2016 (Office of Water Prediction 2019), requiring the use of a HEC-HMS model to model contributing subwatersheds and provide input streamflows as boundary conditions for the 2D hydrodynamic model. The inflow boundary conditions and input rainfall data were obtained from the NWM for this run to mimic a real-time flood forecasting scenario and had a coarse temporal resolution of 1 h compared to the rainfall data set used for modeling Hurricane Matthew. The outlet boundary conditions were assumed not to be influenced by tidal conditions and water backflows associated with tides. The rainfall data obtained from the NWM have a spatial resolution of 500 m. The modeled water elevations were compared to observed water elevations collected from the available USGS stations to demonstrate the model's performance. Both local machines and the Google Cloud Platform (GCP) were used as computational resources to run the model.

Comparison to Observed Conditions

Streamflow, along with unpublished, provisional water elevation data for the stations in the study region, were obtained from USGS (Fig. 1; Table 5). A basic QC was performed on USGS water elevation observation data before using the data to compare with the

TUFLOW model predictions. Water depth observations for each station were converted to a water elevation estimation using the gauge's elevation and vertical datum. The NOAA VDatum tool (NOAA 2019) was used to convert the water elevations into the vertical datum used within the TUFLOW model (NAVD88). Finally, a Python script was written to automate the comparison of the gauge water elevations to the model-predicted water elevations.

The modeled streamflow was compared to the observed streamflow available for nine USGS stations in the study area as an initial model evaluation. To extract the predicted flow from the TUFLOW model, a polyline feature was defined in GIS across the floodplain at each USGS station. The length of this polyline covered the entire floodplain, and not just the bank-full width of the stream, in order to extract the streamflow from the TUFLOW model. If this was not done correctly, the model-predicted streamflow would not represent the total streamflow at the gauging location for that flood event, and, therefore, would likely be a poor match with the observed streamflow time series.

Improvements to the model's predictive skill were quantified as a reduction in the RE between observed and modeled water elevation peaks and improvement in the model's NSE. Watershed-scale models at the spatial and temporal resolution of the TUFLOW simulations are considered to be accurate when the NSE values are at least 0.5 (Moriasi et al. 2007, 2015; Ritter and Muñoz-Carpena 2013).

Results and Discussion

Results from Data Enhancements

Fig. 3 shows results from the four different model versions comparing modeled to observed water elevation at nine different observational stations during Hurricane Matthew. Table 6 gives the water elevation RE and NSE for each station and version of the model. The results show that, after including the high-resolution DEM,

Table 5. Water depth data availability at USGS stations within the study domain

		USGS station			
ID	Station number	Station name	Start	End	
OS-A	02045500	NOTTOWAY RIVER NEAR STONY CREEK, VIRGINIA	October 1, 2003	Current date	
OS-B	02047000	NOTTOWAY RIVER NEAR SEBRELL, VIRGINIA	October 1, 2002	Current date	
OS-C	02052000	MEHERRIN RIVER AT EMPORIA, VIRGINIA	October 1, 2003	Current date	
OS-D	02052090	MEHERRIN RIVER NEAR BRYANTS CORNER, VIRGINIA	November 26, 2012	Current date	
OS-E	02047500	BLACKWATER RIVER NEAR DENDRON, VIRGINIA	October 1, 2003	Current date	
OS-F	02047783	BLACKWATER RIVER AT ROUTE 620 NEAR ZUNI, VIRGINIA	April 25, 2013	Current date	
OS-G	02049500	BLACKWATER RIVER NEAR FRANKLIN, VIRGINIA	October 1, 2007	Current date	
OS-H	02050000	BLACKWATER RIVER AT HWYS 58/258 AT FRANKLIN, VIRGINIA	June 30, 2010	Current date	
OS-I	02047370	NOTTOWAY RIVER NEAR RIVERDALE, VIRGINIA	July 11, 2013	Current date	
OS-J	02053200	POTECASI CREEK NEAR UNION, NORTH CAROLINA	October 1, 2007	Current date	
OS-K	02051500	MEHERRIN RIVER NEAR LAWRENCEVILLE, VIRGINIA	October 1, 2002	Current date	
OS-L	02051000	NORTH MEHERRIN RIVER NEAR LUNENBURG, VIRGINIA	October 1, 2003	Current date	
OS-M	02044500	NOTTOWAY RIVER NEAR RAWLINGS, VIRGINIA	October 1, 2003	Current date	
OS-N	02046000	STONY CREEK NEAR DINWIDDIE, VIRGINIA	October 1, 2003	Current date	

modified streamlines, high-resolution land cover, and road network data sets, the model predictions better fit with the observed water elevation peaks. The model predictions for modeled water elevation were significantly improved for five of the nine USGS stations (OS-A, OS-B, OS-D, OS-E, and OS-F). The RE improved from -9% to 18% in the original model to -1.4% to 7% in the new data set model. There was also a noticeable improvement for the NSE values at all stations except OS-A.

Although the majority of the stations improved after applying the new data set, the model still had poor accuracy at the three stations located on the southeast portion of the model domain (OS-G, OS-H, and OS-I), as shown in Fig. 3 and Table 6. These three stations are located in the lowest-relief region in the study domain, where it is hard to extract the correct bathymetric features of rivers (i.e., river bed elevation and width), even with the use of a high-resolution lidar-derived DEM data set. Thus, these stations highlight the need for bathymetry and cross-section information in low-relief regions.

The model performed as well as or better than the new data set run at most of the USGS stations with cross-section data collected through the site visits described in the section "Channel Cross Section." This improvement made the most substantial difference for the stations located in the low-relief regions of the model domain (OS-G, OS-H, and OS-I). These results show that obtaining accurate cross-sectional data was very important for low-relief terrains and can significantly enhance model performance.

When enhanced rainfall data were used, there were significant improvements to the modeled hydrographs at the USGS stations OS-B, OS-G, OS-H, and OS-I. This improvement suggests that the gridded rainfall data generated from using the gauged rainfall instead of TRMM data provide a better representation of the study region's rainfall, especially for the subbasins draining to these USGS stations. Most of the rainfall came from four NOAA gauges (RG-B, RG-C, RG-G, and RG-H) that are located primarily in the eastern half of the study domain, thereby improving the accuracy of these difficult-to-model, low-relief subbasins.

Finally, the model's ability to predict flow accurately was tested. Fig. 4 compares streamflow hydrographs between the modeled and observed discharge for the final model version during Hurricane Matthew. Except for OS-E and OS-B, all the USGS stations

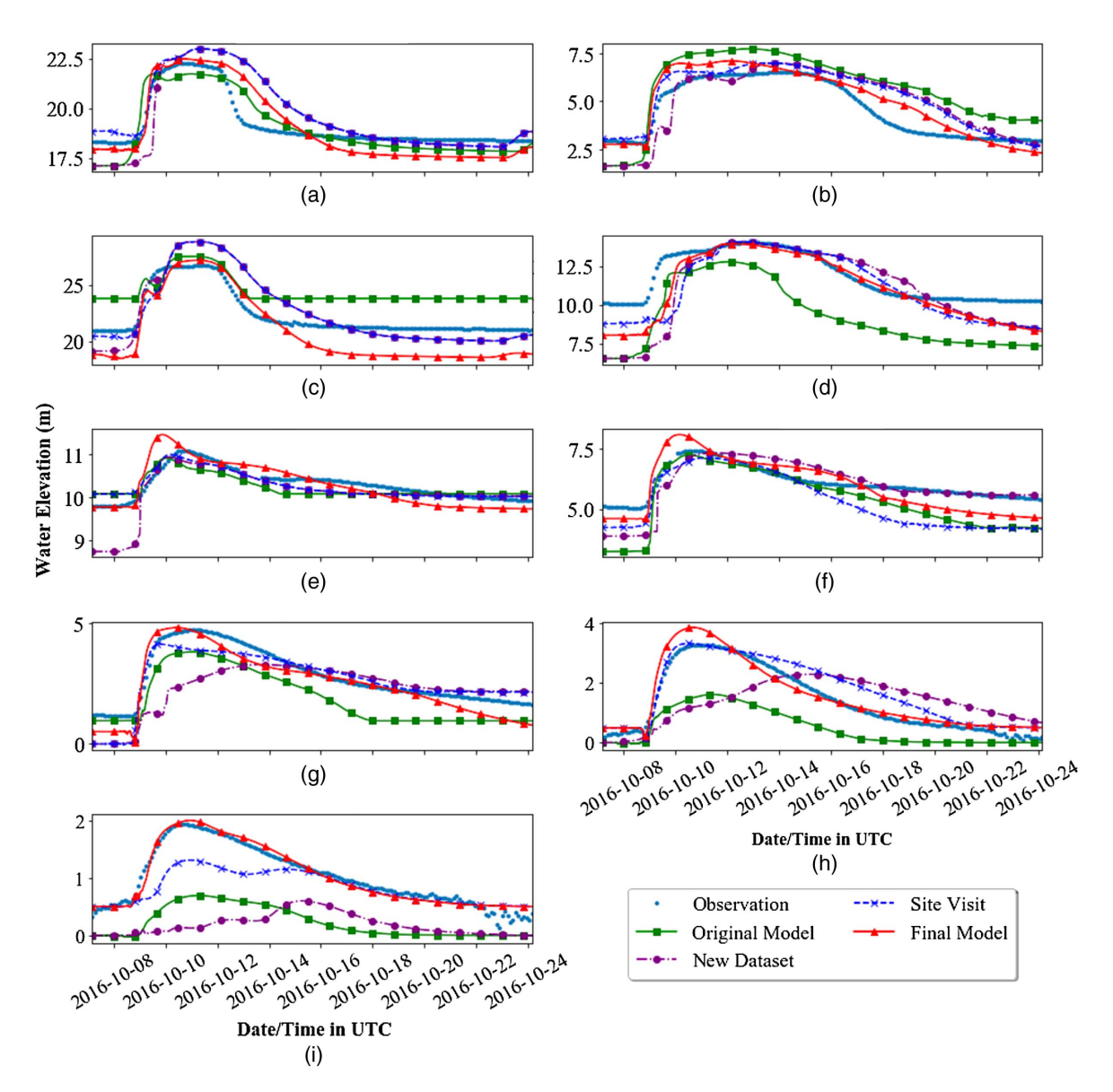


Fig. 3. Model output for the four data enhancement versions at nine USGS stations for Hurricane Matthew: (a) OS-A; (b) OS-B; (c) OS-C; (d) OS-D; (e) OS-E; (f) OS-F; (g) OS-G; (h) OS-H; and (i) OS-I.

modeled streamflow that approximately matches the observed discharge with RE values ranging from -10.81% to 10.56% and NSE values ranging from 0.72 to 0.95. Overall, this comparison to discharge provides further evidence that the model has predictive skill in that it can simulate streamflow resulting from Hurricane Matthew accurately.

Discussion of Data Enhancements

This work started with the original model with an average RE and NSE of -14.21% and 0.39, respectively. In the first phase of the model enhancement, higher-resolution terrain data, streamline representations, land cover data, and road network data sets were carefully combined to improve the underlying geospatial framework used to generate the model input files. With these changes, the average RE and NSE were reduced slightly to -12.59% and 0.23, respectively. These time-consuming efforts to improve the model, arguably, did not justify the effort.

In the second phase of the model enhancement, site visits were performed at select locations in the region to obtain surveyed crosssection data to improve the model's bathymetric representation. As a result, there was a significant improvement in the model performance, especially for the model's low-relief areas. The average RE was reduced to -3.29%, and the NSE improved to 0.56, which is within the acceptable range of a well-calibrated model according to established guidelines (McCuen et al. 2006; Moriasi et al. 2007, 2015; Ritter and Muñoz-Carpena 2013). Some work has focused on estimating river bathymetry using standard geometric shapes due to the lack of widely available river bathymetric data and the computational demands of using such data (Grimaldi et al. 2018). However, results from the data enhancements in this study indicate that the model is sensitive to channel bathymetry relative to other inputs, especially within the study region's low-relief portion. Consequently, future work should focus on improving river bathymetric representation within the model.

In the final phase of the model enhancement, rainfall representation was improved by using NOAA gauges. The QC measures taken for this phase of model enhancements allowed for outliers and stations that had malfunctioned during the studied storm event to be removed. These outliers and malfunctions could have led to increased or reduced rainfall amounts. Thus, with their removal, the rainfall distribution created had a more accurate representation of rainfall in the study domain. These final adjustments led to an average RE of 5.15% and an average NSE of 0.67. These results suggest that, in addition to pursuing bathymetric representation improvements, future research should also work to improve rainfall inputs and representations within the study domain.

Model Evaluation

Figs. 5 and 6 show the modeled water elevation for the October 11, 2018, event using observed rainfall and inflow boundary condition time series. For stations in the higher-relief portion of the study domain (Fig. 5), the model results for water elevation estimates can be considered acceptable at Stations OS-A, OS-B, OS-C, and OS-D with RE values of -0.58%, 2.04%, 1.42%, and 0.67%, respectively, and NSE values of 0.76, 0.24, 0.51, and 0.43, respectively. The model in its current state could be used for flood forecasting of less extreme events within this higher-relief portion of the watershed.

While the model performed well for stations in the higher-relief portion of the study domain (OS-A through OS-D), it did not perform as well for stations in the lower-relief portion (OS-E through OS-I) (Fig. 6). Station OS-E had an RE of 9.75% with a low NSE

value of -0.86. Station OS-I, which is located near the outlet of the 2D model, had an RE value of 47.53% and a low NSE value of -0.32. Similarly, Stations OS-F, OS-G, and OS-H performed poorly. It can be seen from the results that the model tended to predict a higher water level than observed at Stations OS-E through OS-I. The model showed that the rivers largely did not respond to the rainfall event at these stations. OS-E through OS-H are part of the same low-relief watershed; thus, it is possible the rainfall in this basin did not match the rainfall used to drive the model. Another possibility is that more channel cross sections and bathymetric information are needed to better characterize this low-relief portion of the study domain. More model testing including with other rainfall events would be needed before the model could be used for flood forecasting within this lower-relief portion of the watershed.

OS-I is located near the outlet of the watershed and includes flow from both the western, higher-relief watershed (with Stations OS-A and OS-B) and eastern, lower-relief watershed (with Stations OS-E through OS-H). Because there was relatively little runoff generated from October 11, 2018 storm event compared to the Hurricane Matthew event, it seems from the observation data at OS-I that tidal effects influenced the lower portion of the catchment during the October 11, 2018 storm event. This tidal influence was not observed in the Hurricane Matthew data, and, as a result, tidal effects were not included in the model. This is most likely due to the larger volume of runoff associated with Hurricane Matthew dominating the flood behavior in the lower, tidally influenced portion of the study area. In addition to highlighting the impacts of the omission of tidal effects, this test run also highlights the impact that relatively coarse, hourly rainfall data can have on the model's performance when applied to a second, independent storm event. Thus, while this test run indicated acceptable model performance for the higher-relief portion of the watershed, it also demonstrated the model's reliance on highquality data, especially in low-relief regions. Therefore, results from this test run suggest other factors, such as improved rainfall observation and channel bathymetric representations, and including downstream boundary conditions such as tidal effects, may need to be included in future iterations of the model if there is a need to simulate flooding impacts from smaller events, like the October 11, 2018, event. These results support Santiago-Collazo et al.'s (2019) findings, which were that downstream boundary conditions must be included for compound flooding due to rainfall-runoff and storm surge in coastal floodplains.

Model Limitations

In addition to these factors, other dynamics may need to be included for the realization that tidal effects may be needed in future versions of the 2D hydrodynamic model. For example, the initial assumption in the model was that the domain was saturated prior to the storm event. For Hurricane Matthew, this was an appropriate assumption. In the days preceding Hurricane Matthew, two significant storm events (Hurricane Hermine on September 3, 2016, and Tropical Storm Julia on September 19, 2016) impacted the study domain. Because the soil was already saturated from these two events, it could be safely assumed that infiltration would not be a dominating process for modeling water surface elevation and discharge for Hurricane Matthew. However, in general, it will be necessary to consider antecedent soil moisture conditions and infiltration processes in the model to enhance the model performance for other events.

For this study, tests were also conducted to determine model sensitivity to groundwater elevation. These results showed that the four groundwater wells available in this large domain are likely unable to

Table 6. Comparison of the modeled and observed water elevation based on the RE and NSE statistics for the four data enhancement versions at nine USGS stations for Hurricane Matthew

	Original model		New data set		Site visit		Final model	
Station ID	Water elevation peak RE (%) NSE		Water elevation peak RE (%)	NSE	Water elevation peak RE (%)	NSE	Water elevation peak RE (%)	NSE
OS-A	-2.41	0.74	3.23	0.5	3.24	0.5	0.99	0.64
OS-B	18.27	0.42	6.97	0.45	7.04	0.73	8.78	0.81
OS-C	3.07	0.39	7.93	0.43	7.94	0.47	1.75	0.4
OS-D	-8.95	0.2	0.35	0.43	0.31	0.35	-0.6	0.5
OS-E	-1.61	0.64	-1.36	0.05	-0.085	0.77	3.31	0.59
OS-F	-2.34	-0.1	-1.22	0.03	-4.12	-0.05	8.98	0.3
OS-G	-19.18	0.55	-30.3	0.12	-12.33	0.8	2.11	0.85
OS-H	-50.66	0.45	-30.1	-0.01	1.43	0.86	17.63	0.94
OS-I	-64.12	0.21	-68.81	0.08	-32.24	0.62	3.38	0.96
Average	-14.21	0.39	-12.59	0.23	-3.29	0.56	5.15	0.67

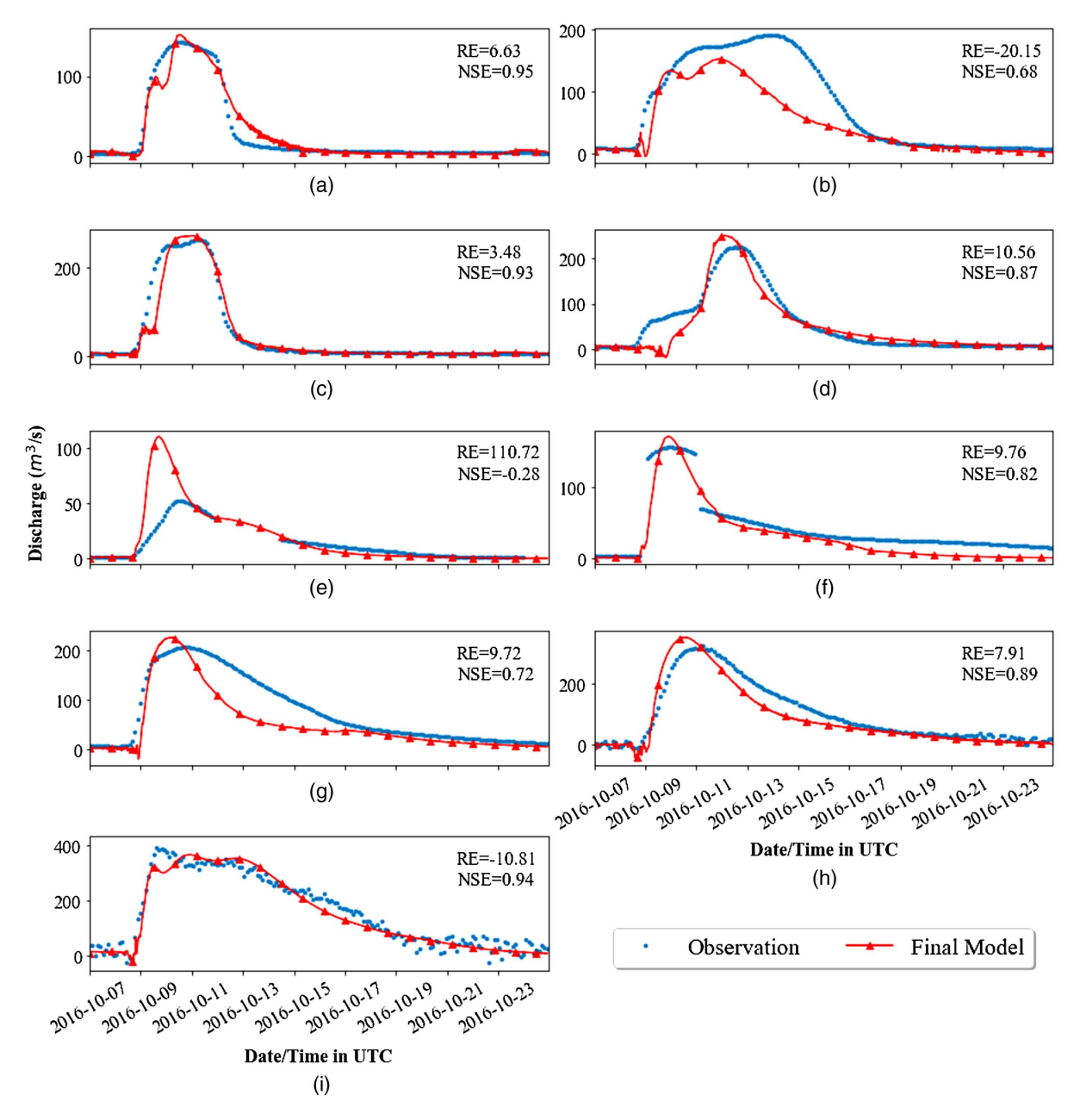


Fig. 4. Final model output for Hurricane Matthew showing the match to discharge observations for USGS stations (a) OS-A; (b) OS-B; (c) OS-C; (d) OS-D; (e) OS-E; (f) OS-F; (g) OS-G; (h) OS-H; and (i) OS-I.

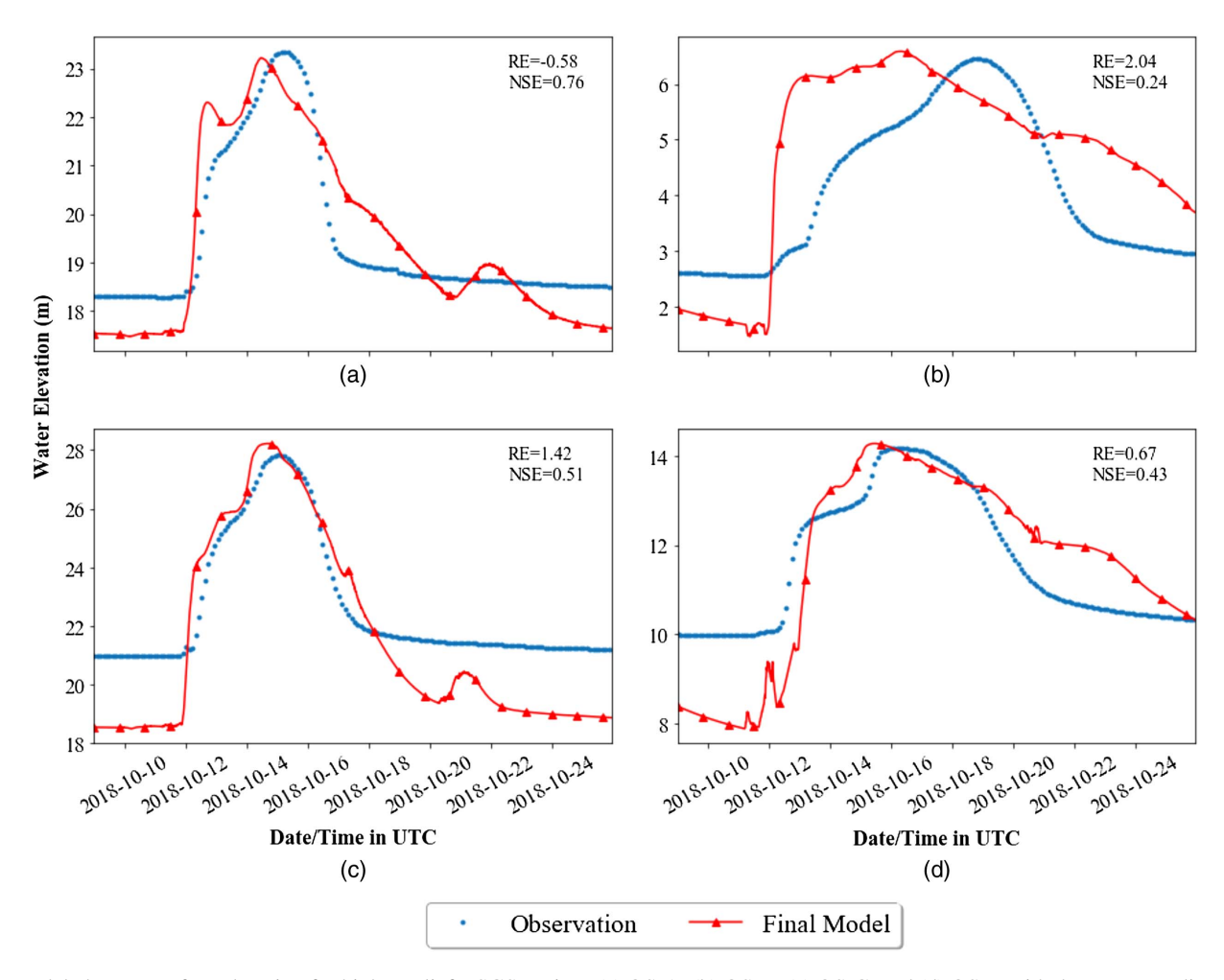


Fig. 5. Modeled water surface elevation for higher-relief USGS stations (a) OS-A; (b) OS-B; (c) OS-C; and (d) OS-D with the corresponding RE and NSE values for the October 11, 2018, storm event used for model evaluation.

capture the real groundwater table variability across the study domain. Assuming a high groundwater table, based on antecedent soil moisture conditions, may be more appropriate for the Hurricane Matthew simulations. For other events, this could be considered a setting in the model that is adjusted based on antecedent rainfall and, perhaps, baseflow conditions before the storm event occurs.

Some locations, particularly those in lower-relief portions of the watershed, may also require a more complex hydrodynamic model that includes factors, like wind and tide, or a finer computational cell resolution than the 30-m fixed-grid resolution used in this study to capture flow dynamics. For instance, Station OS-F had the lowest water elevation NSE value of 0.3, but still showed a significant improvement compared to the original model, new data set, and site visit runs. This station's location has tremendous amounts of storage within its broad floodplain. Routing water through these systems is not as straightforward because sometimes the water flows out into floodplain storage and then back into the channel as the system drains, and sometimes it will flow upstream due to wind and tide. These complications could be a source of the errors affecting Station OS-F and could be improved with a more complex hydrodynamic model that.

Conclusions

This study's primary objective was to understand the effect of input data quality on model accuracy for a regional-scale 2D

hydrodynamic model implemented in a low-relief coastal plain. The goal of this study was not to produce a fully calibrated and validated flood forecasting model but rather to understand how various enhancements to underlying geospatial data used by the model contribute to the accuracy of water level predictions. The study results, therefore, are recommendations for which data enhancements should be prioritized for similar 2D hydrodynamic modeling efforts given often limited resources in creating such models and their significant runtime that limit the ability to perform a thorough model calibration and validation. Building from a model described in Morsy et al. (2018), data enhancements to the model explored through this study were divided into three phases, or versions of the model. In the first phase, the original topographical and land use information were replaced with data sets of a higher resolution, and streamlines in the model were updated to match the new high-resolution topography, areal imagery, and NHDPlus streamlines. In the second phase, detailed, ground-truthed crosssectional data for major rivers near USGS sites in the study domain's low-relief portion were added. In the third phase, rainfall data were put through improved QC procedures before being used in the model. After each phase, improvements to the model were quantified as a reduction in the RE between observed and modeled water elevation and improvement in the model's NSE.

The study results suggest that only having high-resolution DEM and land use data sets to build a 2D hydrodynamic model for detailed flood predictions will likely be insufficient in low-relief coastal plain regions. Instead, accurate channel cross-sectional

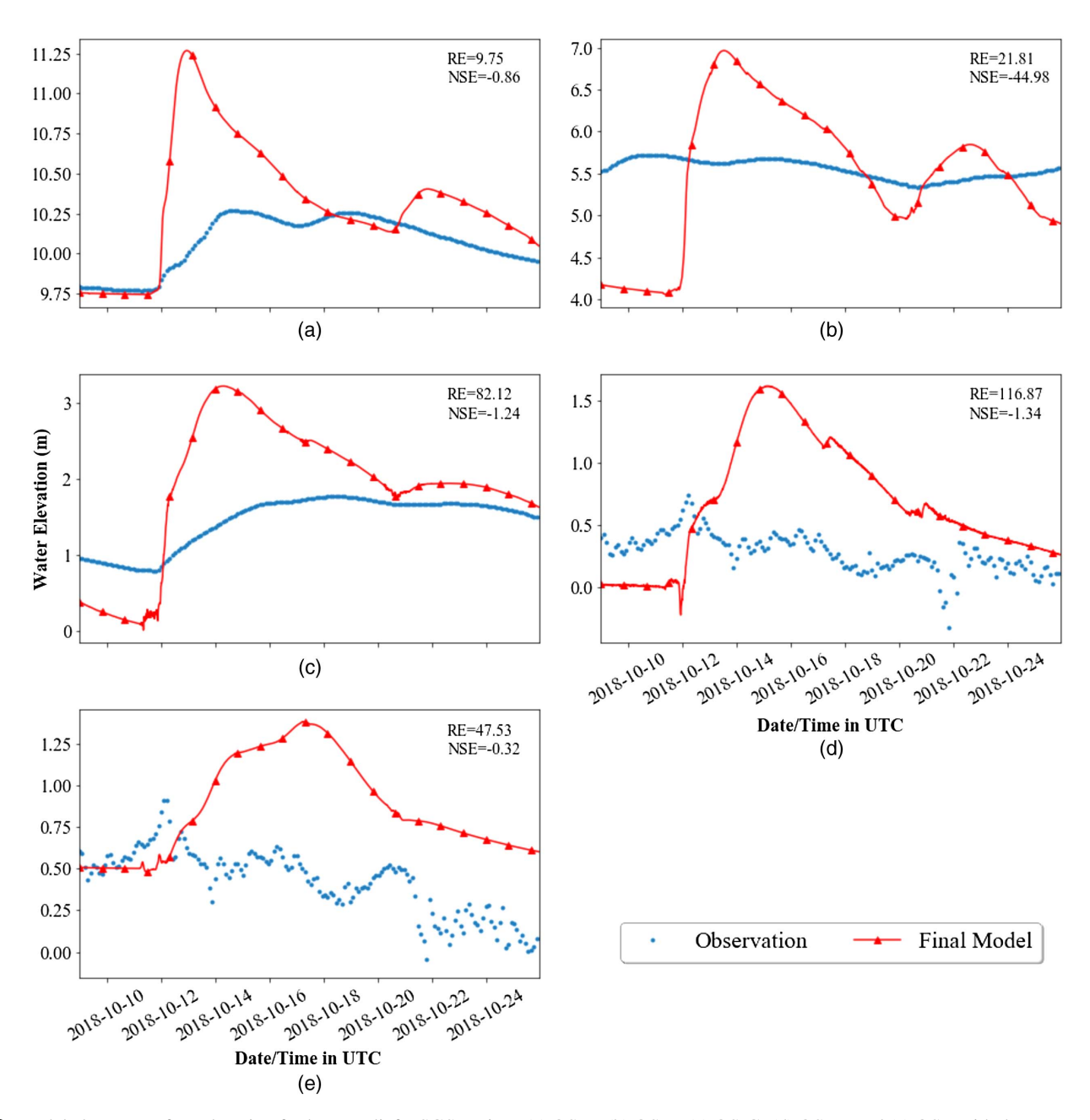


Fig. 6. Modeled water surface elevation for lower-relief USGS stations (a) OS-E; (b) OS-F; (c) OS-G; (d) OS-H; and (e) OS-I with the corresponding RE and NSE values for the October 11, 2018, storm event used for model evaluation.

data, not derived from a high-resolution DEM but through site visits to capture the river bathymetry, was the most critical of the tested factors in achieving an accurate model. Additionally, this analysis reinforced how QC methods for observed rainfall data were critical for flood prediction, given how rain gauges can malfunction during extreme rainfall events. Many of the rainfall gauging locations encountered errors during Hurricane Matthew and needed to be excluded from the analysis due to mechanical faults with the stations during this extreme event. Including these data without a thorough QC would increase error in the model that no amount of enhancements and calibration can overcome. Thus, this study suggests that additional focus should be placed both on (1) improved collection and integration of river bathymetry with topographic data for lowrelief coastal plains, and (2) improved methods for QC of observed rainfall data that can detect faulty stations during extreme rainfall events.

In addition to these suggestions, the model results suggest that future work may also need to include downstream tidal boundary conditions, especially for events like the October 11, 2018, event that had less rainfall, causing tidal boundary conditions to pay a more major role near the outlet of the watershed. As previously mentioned, these gauges near the outlet of the study domain experienced significant tidal effects during the October 11, 2018, event, while the rainfall was less than that of the Hurricane Matthew event used for model calibration. The inclusion of tidal boundary conditions at the ocean-river interface is possible in hydrodynamic models like TUFLOW used in this study as a stage observation at the watershed outlet; however, velocity measurements would be ideal to simulate the propagation of momentum upstream from the tidal forces. Similar to the techniques employed by Bilskie and Hagen (2018) for defining flood zone transitions, transects across the study area may help identify where dominant flood-driving mechanisms transition from hydrologic to coastal (e.g., tidal) within this study area for various storm events.

The computational demands of 2D hydrodynamic models, despite the ability to use multiple GPUs in parallel as was done in this study, remains a significant challenge. While 230 model runs were conducted in this study, each model run still took approximately 10 h to complete, limiting the variety of model alternatives that could be tested. Additional opportunities for speeding up simulations should be explored in future work, such as new approaches for representing spatial heterogeneity in the model like quadtree multidomains. A newly released version of the TUFLOW hydrodynamic model used in this study now includes quadtree functionality and subgrid sampling, which will help to further speed up 2D hydrodynamic models for flood warning applications. With quadtree multidomains, a finer resolution of computational grid cell size can be used in rivers and floodplains where high resolution is necessary, and coarse resolution can be applied to other regions in the model domain. Future research should explore this new capability to test a larger number of model alternatives and further advance approaches for generating accurate, high-resolution flood forecasting information to support decision makers.

Data Availability Statement

Some or all data, models, or code that support the findings of this study are available from the corresponding author upon reasonable request.

Acknowledgments

This work was supported by the Virginia Transportation Research Council (VTRC). We wish to thank Russel Lotspeich from the US Geological Survey for his assistance in obtaining unpublished water elevation data for our study region. We also would like to acknowledge the Viz Lab, a facility for University of Virginia, for providing us with GPU workstations.

References

- Abdullah, A. F., Z. Vojinovic, R. K. Price, and N. A. A. Aziz. 2012. "A methodology for processing raw LiDAR data to support urban flood modelling framework." *J. Hydroinf*. 14 (1): 75–92. https://doi.org/10.2166/hydro.2011.089.
- Bacopoulos, P. 2019. "Extreme low and high waters due to a large and powerful tropical cyclone: Hurricane Irma (2017)." *Nat. Hazards* 98 (3): 939–968. https://doi.org/10.1007/s11069-018-3327-7.
- Bates, P. D., M. G. Anderson, L. Baird, D. E. Walling, and D. Simm. 1992. "Modelling floodplain flows using a two-dimensional finite element model." *Earth Surf. Process. Landf.* 17 (6): 575–588. https://doi.org/10 .1002/esp.3290170604.
- Bates, P. D., and A. P. J. De Roo. 2000. "A simple raster-based model for flood inundation simulation." *J. Hydrol.* 236 (1–2): 54–77. https://doi. org/10.1016/S0022-1694(00)00278-X.
- Bates, P. D., K. J. Marks, and M. S. Horritt. 2003. "Optimal use of high-resolution topographic data in flood inundation models." *Hydrol. Process.* 17 (3): 537–557. https://doi.org/10.1002/hyp.1113.
- Bedient, P. B., W. C. Huber, and B. E. Vieux. 2008. *Hydrology and flood-plain analysis*. 4th ed. Upper Saddle River, NJ: Prentice Hall.
- Bilskie, M. V., and S. C. Hagen. 2018. "Defining flood zone transitions in low-gradient coastal regions." *Geophys. Res. Lett.* 45 (6): 2761–2770. https://doi.org/10.1002/2018GL077524.
- BMT WBM. 2016. *TUFLOW user manual: Build 2016-03-AA*. Brisbane, Australia: BMT Commercial Australia.

- Bruni, G., R. Reinoso, N. C. Van De Giesen, F. H. L. R. Clemens, and J. A. E. Ten Veldhuis. 2015. "On the sensitivity of urban hydrodynamic modelling to rainfall spatial and temporal resolution." *Hydrol. Earth Syst. Sci.* 19 (2): 691–709. https://doi.org/10.5194/hess-19-691 -2015
- Chow, V. T. 1959. *Open-channel hydraulics*. New York: McGraw-Hill. Cobby, D. M., D. C. Mason, and I. J. Davenport. 2001. "Image processing of airborne scanning laser altimetry data for improved river flood mod-
- of airborne scanning laser altimetry data for improved river flood modeling." *ISPRS J. Photogramm. Remote Sens.* 56 (2): 121–138. https://doi.org/10.1016/S0924-2716(01)00039-9.
- Crowder, D. W., and P. Diplas. 2000. "Using two-dimensional hydrodynamic models at scales of ecological importance." *J. Hydrol.* 230 (3–4): 172–191. https://doi.org/10.1016/S0022-1694(00)00177-3.
- Engineers Australia. 2012. "Australian rainfall and runoff revision projects PROJECT 15 two dimensional modelling in urban and rural floodplains STAGE 1&2 REPORT." Accessed December 4, 2018. http://arr.ga.gov.au/_data/assets/pdf_file/0019/40573/ARR_Project15_TwoDimensional_Modelling_DraftReport.pdf.
- Feng, Z., L. R. Leung, S. Hagos, R. A. Houze, C. D. Burleyson, and K. Balaguru. 2016. "More frequent intense and long-lived storms dominate the springtime trend in central US rainfall." *Nat. Commun.* 7 (1): 1–8. https://doi.org/10.1038/ncomms13429.
- Fernandez-Diaz, J. C., C. L. Glennie, W. E. Carter, R. L. Shrestha, M. P. Sartori, A. Singhania, C. J. Legleiter, and B. T. Overstreet. 2014. "Early results of simultaneous terrain and shallow water bathymetry mapping using a single-wavelength airborne LiDAR sensor." *IEEE J. Sel. Top. Appl. Earth Obs. Remote Sens.* 7 (2): 623–635. https://doi.org/10.1109/JSTARS.2013.2265255.
- García, L., J. Barreiro-Gomez, E. Escobar, D. Téllez, N. Quijano, and C. Ocampo-Martinez. 2015. "Modeling and real-time control of urban drainage systems: A review." Adv. Water Resour. 85 (Nov): 120–132. https://doi.org/10.1016/j.advwatres.2015.08.007.
- Giese, G. L., H. B. Wilder, and G. G. Parker. 1985. *Hydrology of major estuaries and sounds of North Carolina*. Alexandria, VA: US GS.
- Grimaldi, S., Y. Li, J. P. Walker, and V. R. N. Pauwels. 2018. "Effective representation of river geometry in hydraulic flood forecast models." Water Resour. Res. 54 (2): 1031–1057. https://doi.org/10.1002 /2017WR021765.
- Horritt, M. S., P. D. Bates, and M. J. Mattinson. 2006. "Effects of mesh resolution and topographic representation in 2D finite volume models of shallow water fluvial flow." *J. Hydrol.* 329 (1–2): 306–314. https:// doi.org/10.1016/j.jhydrol.2006.02.016.
- Kalyanapu, A. J., S. J. Burian, and T. N. Mcpherson. 2009. "Effect of land use-based surface roughness on hydrologic model output." *J. Spatial Hydrol.* 9 (2): 51–71.
- Kalyanapu, A. J., S. Shankar, E. R. Pardyjak, D. R. Judi, and S. J. Burian. 2011. "Assessment of GPU computational enhancement to a 2D flood model." *Environ. Modell. Software* 26 (8): 1009–1016. https://doi.org /10.1016/j.envsoft.2011.02.014.
- Knebl, M. R., Z. L. Yang, K. Hutchison, and D. R. Maidment. 2005. "Regional scale flood modeling using NEXRAD rainfall, GIS, and HEC-HMS/RAS: A case study for the San Antonio River Basin summer 2002 storm event." *J. Environ. Manage*. 75 (4): 325–336. https://doi.org/10.1016/j.jenvman.2004.11.024.
- Lamb, R., M. Crossley, and S. Waller. 2009. "A fast two-dimensional flood-plain inundation model." *Proc. Inst. Civ. Eng. Water Manage*. 162 (6): 363–370. https://doi.org/10.1680/wama.2009.162.6.363.
- Leandro, J., A. S. Chen, S. Djordjević, and D. A. Savić. 2009. "Comparison of 1D/1D and 1D/2D coupled (sewer/surface) hydraulic models for urban flood simulation." *J. Hydraul. Eng.* 135 (6): 495–504. https://doi.org/10.1061/(ASCE)HY.1943-7900.0000037.
- Lim, N. J., and S. A. Brandt. 2019. "Flood map boundary sensitivity due to combined effects of DEM resolution and roughness in relation to model performance." *Geomatics Nat. Hazards Risk* 10 (1): 1613–1647. https:// doi.org/10.1080/19475705.2019.1604573.
- Liu, Z., V. Merwade, and K. Jafarzadegan. 2019. "Investigating the role of model structure and surface roughness in generating flood inundation extents using one- and two-dimensional hydraulic models." *J. Flood Risk Manage*. 12 (1): e12347. https://doi.org/10.1111/jfr3.12347.

- Marks, K., and P. Bates. 2000. "Integration of high-resolution topographic data with floodplain flow models." *Hydrol. Process.* 14 (11–12): 2109–2122. https://doi.org/10.1002/1099-1085(20000815/30)14:11/12<2109:: AID-HYP58>3.0.CO;2-1.
- McCuen, R. H., Z. Knight, and A. G. Cutter. 2006. "Evaluation of the Nash–Sutcliffe efficiency index." *J. Hydrol. Eng.* 11 (6): 597–602. https://doi.org/10.1061/(ASCE)1084-0699(2006)11:6(597).
- McKean, J., D. Isaak, and W. Wright. 2009. "Improving stream studies with a small-footprint green lidar." *EOS Trans. Am. Geophys. Union* 90 (39): 341–342. https://doi.org/10.1029/2009EO390002.
- Medeiros, S. C., S. C. Hagen, and J. F. Weishampel. 2012. "Comparison of floodplain surface roughness parameters derived from land cover data and field measurements." *J. Hydrol.* 452–453 (Jul): 139–149. https://doi .org/10.1016/j.jhydrol.2012.05.043.
- Moriasi, D. N., J. G. Arnold, M. W. Van Liew, R. L. Bingner, R. D. Harmel, and T. L. Veith. 2007. "Model evaluation guidelines for systematic quantification of accuracy in watershed simulations." *Trans. ASABE* 50 (3): 885–900. https://doi.org/10.13031/2013.23153.
- Moriasi, D. N., M. W. Gitau, N. Pai, and P. Daggupati. 2015. "Hydrologic and water quality models: Performance measures and evaluation Criteria." *Trans. ASABE* 58 (6): 1763–1785. https://doi.org/10.13031/trans .58.10715.
- Morsy, M. M., J. L. Goodall, G. L. O'Neil, J. M. Sadler, D. Voce, G. Hassan, and C. Huxley. 2018. "A cloud-based flood warning system for forecasting impacts to transportation infrastructure systems." *Environ. Modell. Software* 107 (Sep): 231–244. https://doi.org/10.1016/j.envsoft.2018.05.007.
- Muñoz, D. F., H. Moftakhari, and H. Moradkhani. 2020. "Compound effects of flood drivers and wetland elevation correction on coastal flood hazard assessment." Water Resour. Res. 56 (7): e2020WR027544. https://doi.org/10.1029/2020WR027544.
- National Research Council. 2009. *Mapping the zone: Improving flood map accuracy*. Washington, DC: National Academies Press.
- NOAA (National Oceanic and Atmospheric Administration). 2013. "Bathy lidar: Harder than it looks: Digital coast GeoZone." Accessed August 10, 2020. https://geozoneblog.wordpress.com/2013/09/25/bathy-lidar -harder-than-it-looks/.
- NOAA (National Oceanic and Atmospheric Administration). 2017. "Extremely active 2017 Atlantic hurricane season finally ends." Accessed May 7, 2020. https://www.noaa.gov/media-release/extremely-active-2017 -atlantic-hurricane-season-finally-ends.
- NOAA (National Oceanic and Atmospheric Administration). 2018. "Historical Hurricane Florence, September 12-15, 2018." Accessed February 28, 2020. https://www.weather.gov/mhx/Florence2018.
- NOAA (National Oceanic and Atmospheric Administration). 2019. "NOAA/NOS vertical datums transformation." Accessed May 29, 2020. https://vdatum.noaa.gov/.
- Noman, N. S., E. J. Nelson, and A. K. Zundel. 2001. "Review of automated floodplain delineation from digital terrain models." *J. Water Resour. Plann. Manage.* 127 (6): 394–402. https://doi.org/10.1061/(ASCE) 0733-9496(2001)127:6(394).
- Ochoa-Rodriguez, S., et al. 2015. "Impact of spatial and temporal resolution of rainfall inputs on urban hydrodynamic modelling outputs: A multi-catchment investigation." *J. Hydrol.* 531 (Dec): 389–407. https://doi.org/10.1016/j.jhydrol.2015.05.035.
- Office of Water Prediction. 2019. "Information about the national water model." Accessed May 13, 2020. https://water.noaa.gov/about/nwm.
- Prein, A. F., C. Liu, K. Ikeda, S. B. Trier, R. M. Rasmussen, G. J. Holland, and M. P. Clark. 2017. "Increased rainfall volume from future convective

- storms in the US." *Nat. Clim. Change* 7 (12): 880–884. https://doi.org/10.1038/s41558-017-0007-7.
- Reynolds, J. E., S. Halldin, J. Seibert, C. Y. Xu, and T. Grabs. 2020. "Robustness of flood-model calibration using single and multiple events." *Hydrol. Sci. J.* 65 (5): 842–853. https://doi.org/10.1080/02626667.2019.1609682.
- Ritter, A., and R. Muñoz-Carpena. 2013. "Performance evaluation of hydrological models: Statistical significance for reducing subjectivity in goodness-of-fit assessments." *J. Hydrol.* 480 (Feb): 33–45. https://doi. org/10.1016/j.jhydrol.2012.12.004.
- Santiago-Collazo, F. L., M. V. Bilskie, and S. C. Hagen. 2019. "A comprehensive review of compound inundation models in low-gradient coastal watersheds." *Environ. Modell. Software* 119 (Sep): 166–181. https://doi.org/10.1016/j.envsoft.2019.06.002.
- Schumann, G., P. Matgen, M. E. J. Cutler, A. Black, L. Hoffmann, and L. Pfister. 2008. "Comparison of remotely sensed water stages from LiDAR, topographic contours and SRTM." ISPRS J. Photogramm. Remote Sens. 63 (3): 283–296. https://doi.org/10.1016/j.isprsjprs .2007.09.004.
- Shrestha, R. R., and F. Nestmann. 2009. "Physically based and data-driven models and propagation of input uncertainties in river flood prediction." *J. Hydrol. Eng.* 14 (12): 1309–1319. https://doi.org/10.1061/(ASCE) HE.1943-5584.0000123.
- Skinner, C., F. Bloetscher, and C. S. Pathak. 2009. "Comparison of NEX-RAD and rain gauge precipitation measurements in South Florida." J. Hydrol. Eng. 14 (3): 248–260. https://doi.org/10.1061/(ASCE)1084-0699(2009)14:3(248).
- SSURGO (Soil Survey Geographic). 2018. Soil survey geographic (SSURGO) database for [Virginia]. Washington, DC: Natural Resources Conservation Service—USDA.
- Steiner, M., J. A. Smith, S. J. Burges, C. V. Alonso, and R. W. Darden. 1999. "Effect of bias adjustment and rain gauge data quality control on radar rainfall estimation." Water Resour. Res. 35 (8): 2487–2503. https://doi.org/10.1029/1999WR900142.
- Tate, E. C., D. R. Maidment, F. Olivera, and D. J. Anderson. 2002. "Creating a terrain model for floodplain mapping." J. Hydrol. Eng. 7 (2): 100–108. https://doi.org/10.1061/(ASCE)1084-0699(2002)7:2(100).
- Timbadiya, P. V., P. L. Patel, and P. D. Porey. 2015. "A 1D–2D coupled hydrodynamic model for river flood prediction in a coastal urban floodplain." J. Hydrol. Eng. 20 (2): 05014017. https://doi.org/10.1061 //ASCE)HE.1943-5584.0001029.
- USGS. 2011. NLCD 2011 land cover (CONUS). Reston, VA: USGS.
- VGIN (Virginia Geographic Information Network). 2016a. "Elevation— LIDAR." Accessed December 4, 2018. https://www.vita.virginia.gov/integrated-services/vgin-geospatial-services/elevation---lidar/.
- VGIN (Virginia Geographic Information Network). 2016b. "Land cover— VITA." Accessed December 4, 2018. https://www.vita.virginia.gov/integrated-services/vgin-geospatial-services/land-cover/.
- Yan, K., A. Tarpanelli, G. Balint, T. Moramarco, and G. Di Baldassarre. 2015. "Exploring the potential of SRTM topography and radar altimetry to support flood propagation modeling: Danube case study." *J. Hydrol.* Eng. 20 (2): 04014048. https://doi.org/10.1061/(ASCE)HE.1943-5584 0001018
- Yu, D. 2010. "Parallelization of a two-dimensional flood inundation model based on domain decomposition." *Environ. Modell. Software* 25 (8): 935–945. https://doi.org/10.1016/j.envsoft.2010.03.003.
- Zhao, L., J. Xia, C. Y. Xu, Z. Wang, L. Sobkowiak, and C. Long. 2013. "Evapotranspiration estimation methods in hydrological models." *J. Geog. Sci.* 23 (2): 359–369. https://doi.org/10.1007/s11442-013-1015-9.